Topological deconfinement transition in QCD at finite isospin density[☆]

Kouji Kashiwa[a], Akira Ohnishi[a]

[a]Yukawa Institute for Theoretical Physics, Kyoto University, Kyoto 606-8502, Japan

Abstract

The confinement-deconfinement transition is discussed from topological viewpoints. The topological change of the system is achieved by introducing the dimensionless imaginary chemical potential (θ). Then, the non-trivial free-energy degeneracy becomes the signal of the deconfinement transition and it can be visualized by using the map of the thermodynamic quantities to the circle S^1 along θ. To understand this "topological" deconfinement transition at finite real quark chemical potential (μ_R), we consider the isospin chemical potential (μ_{iso}) in the effective model of QCD. The phase diagram at finite μ_{iso} is identical with that at finite μ_R outside of the pion-condensed phase at least in the large-N_c limit via the well-known orbifold equivalence. In the present effective model, the topological deconfinement transition does not show a significant dependence on μ_{iso} and then we can expect that this tendency also appears at small μ_R. Also, the chiral transition and the topological deconfinement transition seems to be weakly correlated. If we will access lattice QCD data for the temperature dependence of the quark number density at finite μ_{iso} with $\theta = 2\pi/3$, our surmise can be judged.

Keywords: QCD phase diagram, Deconfinement transition, Complex chemical potential

1. Introduction

Understanding the confinement-deconfinement transition is one of the important subjects in the particle and nuclear physics. In the heavy quark mass limit, the Polyakov loop respecting the gauge invariant holonomy characterizes the deconfinement transition. In that case, the spontaneous $\mathbb{Z}_3$ symmetry breaking describes the deconfinement transition and the Polyakov-loop becomes the order parameter of the symmetry breaking. On the other hand, the Polyakov loop cannot be considered as the order-parameter of the deconfinement transition at finite quark mass.

Recently, it was found that the confined and deconfined states at zero temperature ($T = 0$) are characterized by the ground-state degeneracy when the system has non-trivial topology [1]. This argument is based on the topological order discussed in the condensed matter physics where the spontaneous symmetry breaking is absent [2]. Thus, we can expect that the deconfinement transition can be described by the topological order and then it does not require spontaneous symmetry breaking. In Ref. [3], the present authors consider the free-energy degeneracy at finite T based on the analogy of the ground-state degeneracy to determine the deconfinement phase transition. The modification of the topology is achieved by introducing the dimensionless imaginary chemical potential, $\theta \equiv \mu_I/T \in \mathbb{R}$ where μ_I is the imaginary chemical potential. As a result, the deconfinement transition temperature at zero real quark chemical potential ($\mu_R = 0$) can be determined by the Roberge-Weiss (RW) endpoint temperature, T_{RW}. The RW endpoint is the endpoint of the RW transition at $\theta = \pi/N_c$ where N_c is the number of

colors [4]. This suggests that the deconfinement transition may be the topological phase transition related with the topological order.

From differences of topology between the confined and deconfined phases as mentioned above, we can construct the quantum order-parameter which we call the quark number holonomy [5] as

$$\Psi = \oint_0^{2\pi} \text{Im}\left(\frac{d\tilde{n}_q}{d\theta}\right) d\theta, \tag{1}$$

where $\tilde{n}_q = n_q/T^3$ represents the quark number density normalized by T^3 to make Ψ dimensionless. When n_q has the gap at $\theta = \pi/N_c$, Ψ should be nonzero and it counts the number of the gapped points of n_q along θ;

$$\Psi = 2N_c \lim_{\epsilon \to 0} n_q\left(\theta = \frac{\pi}{N_c} - \epsilon\right). \tag{2}$$

Therefore, $\theta = \pi/N_c$ is an important and interesting point. If the RW endpoint becomes the triple-point where three first-order transition lines meet [6, 7], the point where Ψ start to have nonzero value is shifted to lower temperature than T_{RW}. This temperature is sometimes called T_{Beard}; see Ref. [5] for details. In both cases, we can see difference of topology between the confined and deconfined phases and thus we can state that the deconfinement transition is the topological phase transition. It should be noted that the expression (1) is valid not only at zero density but also finite density.

The topological structure can be visualized via the map of thermodynamic quantities, for example the thermodynamic potential, to the circle S^1 along periodic θ as shown in Fig. 1. Here, we plot the thermodynamic states which are global mini-
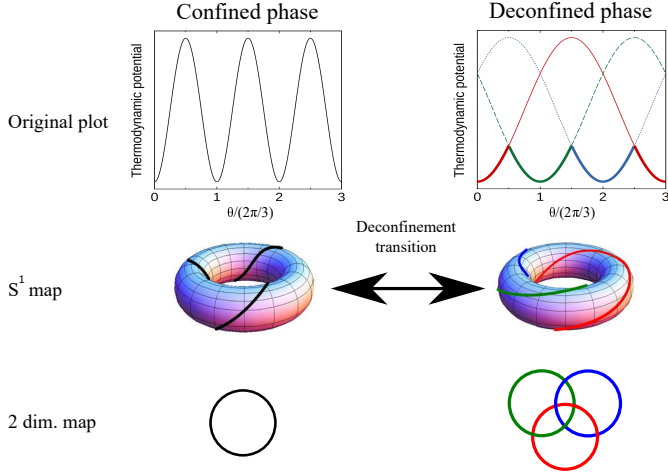
Figure 1: Schematic figures of the topological difference in the confined and deconfined phases with $N_c = 3$. The left (right) column represents the confined (deconfined) phase. The first, second and third rows are the original θ-dependence of the thermodynamic potential, its map to S^1 and its map to 2 dimensional space by replacing the torus. In the right panel of the first row, the bold line represents the global minima. In the second row, solid lines which wind around torus are realized thermodynamic state (global minima of the effective potential) and its $\mathbb{Z}_3$ images if those exist.

mum and two possible local minima of the thermodynamic potential at each θ as lines on the torus. Two possible local minima are so called the $\mathbb{Z}_3$ images of the global minimum. In the confined phase, only one line winds around the torus N_c times, but there are N_c lines in the deconfined phase and each line wind around the torus only one time. Number of winding are related with the RW periodicity and its realization mechanism [4, 3]. By removing the torus, lines can be mapped to the 2-dimensional space as closed rings: one ring exists in the confined phase and three entangled rings appear in the deconfined phase. These entangled rings are not the Borromean rings because we cannot untangle them by removing one ring.

To see more topological properties of thermodynamic states, we consider three operations, Θ, Υ and $\mathbb{Z}_{N_c}$, for the thermodynamic state. We set the global minimum of the thermodynamic potential at $\theta = 0$ as the initial thermodynamic state and express it as $\psi(\theta = 0, \phi = 0)$ where ϕ represents the phase of the Polyakov loop. In the case with $N_c = 3$, ϕ can take $0, 2\pi/3$ and $4\pi/3$ in the deconfined phase. Three operations are following: (Θ operation) It shifts $\psi(\theta, \phi)$ to $\psi(\theta + 2\pi, \phi')$ and then we trace the state which thermodynamic potential decreases if states intersect each other when θ is varying. (Υ operation) It shifts $\psi(\theta, \phi)$ to $\psi(\theta + 2\pi/N_c, \phi)$. It can be interpreted that the certain flux is inserted to the closed Euclidean temporal coordinate loop and then θ is shifted by the Aharonov-Bohm effect. ($\mathbb{Z}_{N_c}$ operation) It is the standard $\mathbb{Z}_{N_c}$ transformation which changes $\psi(\theta, \phi)$ to $\psi(\theta, \phi + 2\pi/N_c)$ if the $\mathbb{Z}_{N_c}$ images exist. In the confined phase, these operations should commute with each other because thermodynamic states at any θ belong to the same image as shown in the left-top panel of Fig. 1. By comparison, three operations are not always commutable in the deconfined phase and these show non-trivial commutation relations.

The topological determination of the deconfinement phase

transition is not yet applied to nonzero μ_R region and thus we investigate this region in this paper by using the effective model approach. At finite μ_R, there is the sign problem in the lattice QCD simulation and thus we cannot obtain reliable results. Therefore, the effective model calculations are important to have qualitative and quantitative understanding of the QCD phase structure. To describe the non-trivial free-energy degeneracy correctly, effective models should possess several topological properties of QCD at finite θ. Such effective models sometimes have the model sign problem [8, 9] which, of course, relates with the original sign problem. The model sign problem can be resolved by using the Lefschetz-thimble path-integral method [10, 11, 12] and then we may investigate μ_R region directly [9], but it is not an easy task at present. We need some more technical extensions of Ref. [9] in the complex μ case.

In this paper, we consider μ_{iso} as an alternative approach to investigate the QCD phase structure at finite μ_R. It is because phase diagrams at finite μ_R and μ_{iso} are identical outside of the pion condensed region in the large-N_c limit via the well-known orbifold equivalence [13, 14, 15].

This paper is organized as follows. In the next section, we explain the isospin chemical potential and formulation of the effective model. Numerical results are shown in Sec. 3 Section 4 is devoted to summary.

2. Effective model with isospin chemical potential

In this paper, we consider μ_{iso} to extract information of the μ_R region because the μ_{iso} region has following two characteristic properties:

1. Sign problem free

It is well known that there is no sign problem because the condition $\tau_2 \gamma_5 \mathcal{D} \gamma_5 \tau_2 = \mathcal{D}^\dagger$ is manifested where $\mathcal{D}$ denotes the Dirac operator and the symbol τ_i mean Pauli matrices in the flavor space. This leads the condition $\det(\mathcal{D}) \geq 0$ even if μ_I is nonzero.

2. Orbifold equivalence

The phase structure at finite μ_{iso} is identical with that at finite μ_R outside of the pion-condensed phase at least in the large-N_c limit [15]. This equivalence is violated with finite N_c by $1/N_c$ corrections such as the flavor mixing loops.

With the two properties, we can expect that the qualitative information of QCD phase diagram at finite μ_R can be extracted from the QCD phase diagram at finite μ_{iso}. For example, the no-go theorem of critical phenomena were obtained in Ref. [16] via the orbifold equivalence. The mean-field approximation which picks up the leading-order of the $1/N_c$ expansion is widely used in the effective model calculation to investigate the QCD phase structure and thus our analysis based on the orbifold equivalence can be acceptable for a first step of the issue to understand the topological deconfinement transition at finite μ_R.

To investigate the phase structure at finite T and μ_{iso}, we use the Polyakov-loop extended Nambu–Jona-Lasinio (PNJL) model [17]. This model can well reproduce the QCD properties

2

at finite θ; see Ref. [18] as an example. The Lagrangian density of the two-flavor and three-color PNJL model in the Euclidean space is

$$\mathcal{L} = \bar{q}(\not{D} + m_0) - G[(\bar{q}q)^2 + (\bar{q}i\gamma_5\vec{\tau}q)^2] + \mathcal{V}_g(\Phi, \bar{\Phi}), \quad (3)$$

where m_0 means the current quark mass, the covariant derivative is $D_\nu - igA_\nu\delta_{\nu4}$, Φ ($\bar{\Phi}$) denotes the Polyakov-loop (its conjugate) and $\mathcal{V}_g$ expresses the gluonic contribution. In the case with $m_0 = \mu_{iso} = 0$, the Lagrangian density has $SU(2)_L \times SU(2)_R \times U(1)_V \times SU(3)_{color}$ symmetry. With $m_0 \neq 0$ and $\mu_I \neq 0$, the Lagrangian density has $U(1)_{I_3} \times U(1)_V \times SU(3)_{color}$ symmetry.

The imaginary and isospin chemical potentials can be introduced to the model as the form

$$\mu = \mu_q\mathbf{I} + \mu_{iso}\tau_3, \quad (4)$$

where $\mathbf{I}$ is the unit matrix. Each μ_q and μ_{iso} can be represented as

$$\mu_q = \frac{\mu_u + \mu_d}{2}, \quad \mu_{iso} = \frac{\mu_u - \mu_d}{2}, \quad (5)$$

where μ_u (μ_d) is the quark chemical potential of up (down) quark. In this paper, we consider $\mu_q = i\mu_I$ ($\mu_I \in \mathbb{R}$) and $\mu_{iso} \in \mathbb{R}$ to discuss the topological deconfinement transition at finite μ_{iso}.

With the mean-field approximation, the thermodynamic potential can be expressed as

$$\mathcal{V} = \mathcal{V}_f + \mathcal{V}_g. \quad (6)$$

where $\mathcal{V}_{f,g}$ are the fermionic and gluonic parts, respectively. The actual form of $\mathcal{V}_f$ is

$$\mathcal{V}_f = -2 \sum_{i=\pm} \int \frac{d^3p}{(2\pi)^3} \Big[3E_{i,\mathbf{p}} + T\ln\big(f_i^- f_i^+\big) \Big]$$
$$+ G(\sigma^2 + \pi^2), \quad (7)$$

where

$$f_i^- = 1 + 3(\Phi + \bar{\Phi}e^{-\beta E_{i,\mathbf{p}}^-})e^{-\beta E_{i,\mathbf{p}}^-} + e^{-3\beta E_{i,\mathbf{p}}^-},$$
$$f_i^+ = 1 + 3(\bar{\Phi} + \Phi e^{-\beta E_{i,\mathbf{p}}^+})e^{-\beta E_{i,\mathbf{p}}^+} + e^{-3\beta E_{i,\mathbf{p}}^+}. \quad (8)$$

Quark single particle energies are given as $E_{\pm\mathbf{p}}^\mp = E_\pm \mp i\mu_I$ with $E_\pm = \sqrt{(E_{\mathbf{p}} \pm \mu_{iso})^2 + N^2}$ for $E_{\mathbf{p}} = \sqrt{\mathbf{p}^2 + M^2}$. Symbols M and N are defined as $M = m_0 - 2G\sigma$ and $N = -2G\pi$ with $\sigma = \langle\bar{q}q\rangle$ and $\pi = \langle\bar{q}i\gamma_5\tau_1q\rangle$. Here we take the order parameter of the $U(1)_{I_3}$ symmetry breaking as

$$\pi^\pm = \frac{1}{\sqrt{2}}e^{\pm i\varphi} = \langle\bar{q}i\gamma_5\tau_\pm q\rangle, \quad (9)$$

and we can set $\varphi = 0$ as in Ref. [19] without loss of generality. In the following disucssions, we set $\pi = |\langle\bar{q}i\gamma_5\tau_1q\rangle|$.

We employ the Polyakov loop potential used in Ref. [20] as $\mathcal{V}_g$ and the parameter set used in Ref. [21]; for details of the PNJL model with μ_{iso}, see Refs. [19, 22, 21] as an example. In

the PNJL model, the *model Polyakov-loop* is defined as

$$\Phi = \frac{1}{N_c}\text{tr}_c\Big[e^{ig\langle A_4\rangle/T}\Big], \quad (10)$$

with the Polyakov-gauge fixing. The Polyakov loop is, of course, gauge invariant, but Eq. (10) is not; see Ref. [23] for discussions on the model and correct Polyakov-loops from the Jensen inequality. Nevertheless, the model Polyakov loop Eq. (10) is enough for our purpose. The Polyakov loop is introduced to just model the $\mathbb{Z}_3$ properties of QCD because the modeling of $\mathbb{Z}_3$ properties plays a crucial role to reproduce characteristic properties of QCD at finite θ. Thus, there is no need to reproduces the correct Polyakov-loop by the model Polyakov-loop. It is the reason why we use the simplest PNJL model in this paper.

3. Numerical results

To investigate the topological deconfinement transition, $\theta = \pi/3$ region is important as shown in Eq. (2) and thus we show the quark number density at $\theta = \pi/3$ in addition to the chiral condensate, the pion condensate and the Polyakov loop at $\theta = 0$ here. Figure 2 shows $|\sigma|/m_\pi^3$, π/m_π^3, $|\Phi|$ and $|n_q|/m_\pi^3$ as a function of T/m_π and μ_{iso}/m_π. The chiral and pion condensates strongly
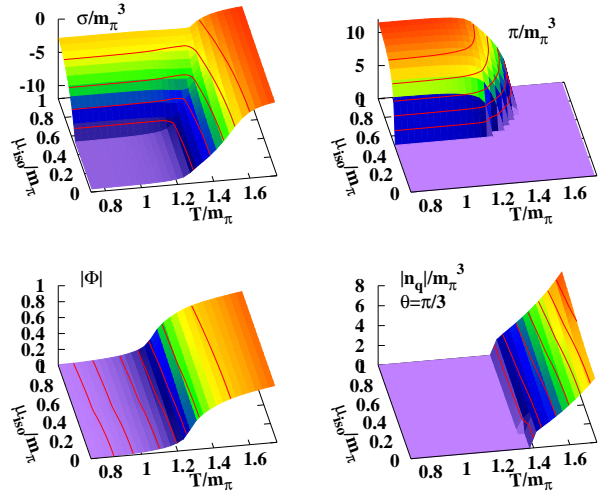

Figure 2: The T and μ_{iso} dependence of the chiral condensate, the pion condensate and the Polyakov loop at $\theta = 0$ and the quark number density at $\theta = \pi/3$. Quantities are normalized by $m_\pi = 138$ [MeV].

depend on μ_{iso} as well as on T, but the Polyakov loop and the quark number density do not. In the leading-order approximation of the PNJL model, the gluonic contributions do not have the explicit chemical-potential dependence because there is no quark polarization effects which are higher order contributions of the $1/N_c$ expansion. Thus, μ_{iso} cannot affect the Polyakov loop directly. Interesting point is that the quark number density is also insensitive to μ_{iso} and it means that the chiral and deconfinement transition are not correlated strongly. This tendency can be expected to appear at finite μ_R via the orbifold equivalence outside of the pion-condensed phase.

For reader's convenience, we show the T/m_π dependence of $|\sigma|/\sigma_0$, π/σ_0 and Φ at $\theta = 0$ and $|n_q|/\sigma_0$ at $\theta = \pi/3$ with $\mu_{iso}/m_\pi = 0, 0.4, 0.6, 1$ in Fig. 3.
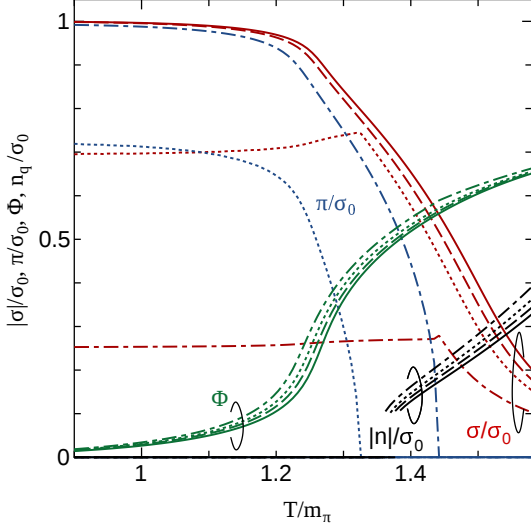

Figure 3: The T dependence of the chiral condensate, the pion condensate and the Polyakov loop at $\theta = 0$ and the quark number density at $\theta = \pi/3$. The solid, dashed, dotted, and dot-dashed lines are these quantities at $\mu_{iso}/m_\pi = 0, 0.4, 0.6,$ and 1, respectively. Quantities are normalized by $\sigma_0 = |\sigma_{vacuum}|$. The step-size of T is 1 [MeV].

The phase diagram in the (T, μ_{iso}) plane is shown in Fig. 4. The solid, dashed, dotted and dot-dashed lines are the de-
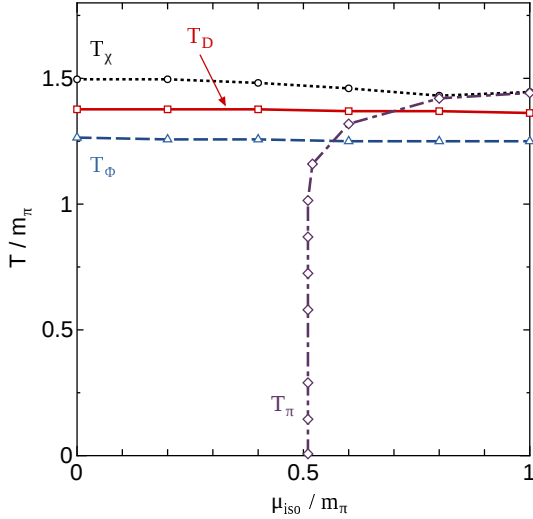

Figure 4: The phase diagram in the T-μ_{iso} plane. Symbols are numerical results and lines are linear interpolations between them. The solid, dashed, dotted and dot-dashed lines are explained in the text. Numerical error of these lines are about ± 1.5 [MeV].

confinement transition temperature (T_D), the deconfinement pseudo-critical temperature determined by the peak of $d\Phi/dT$ (T_Φ), the chiral pseudo-critical temperature determined by the peak of $d\sigma/dT$ (T_χ) and the phase transition temperature of the pion condensation (T_π). If $d\sigma/dT$ and $d\Phi/dT$ have two peaks, we choice higher one as the pseudo-critical temperature. We

determine T_D by T_{RW} in this paper because the triple-point nature of the RW endpoint depends on the form of $\mathcal{V}_g$ in the PNJL model and also the qualitative behavior of T_{RW} and T_{Beard} are basically same. From Fig. 4, we can find following features:

1. Behavior of T_D and T_Φ

T_D and T_Φ slightly decrease with increasing μ_{iso} and show similar qualitative behaviors. However, Φ is continuously changed at finite T and thus the determination of T_Φ is not clear unlike T_D.

2. Behavior of T_D at finite density

T_D decreases with increasing μ_{iso} and thus we can expect that T_D also show decreasing behavior at finite μ_R via the orbifold equivalence. This result is consistent with our perturbative estimate of T_D at small μ_R [3].

3. Relation between T_D and T_χ

The present definition of T_D is not affected much by the chiral transition even though we use the quark-bilinear $\langle q^\dagger q \rangle$.

4. Relation between T_D and T_π

By comparison, T_D seems to be smaller than T_π at large μ_{iso}. This is not unreasonable since these transition are independent of each other. Finite quark mass leaves σ finite and pion keeps its Nambu-Goldstone boson nature even at large T. For example, some effective model results including the present one show $T_\chi > T_D$ at $\mu_R = 0$.

We also note that T_D is smaller than T_χ at small μ_{iso}. When the pseudo-critical chiral transition boundary ends at the RW endpoint, one should find $T_\chi(\theta = 0) < T_\chi(\theta = \pi/3) = T_{RW}(= T_D)$. It should be noted that this is not always the case; the order of two temperatures, T_χ and T_{RW}, depends on the details of the framework. In the present setup, the chiral transition boundary reaches the RW transition line ($\theta = \pi/3$) at significantly higher temperature than the RW endpoint, $T_\chi(\theta = \pi/3) > T_{RW}$.

Sensitivity of the critical temperature on the chemical potential is quantified using the curvature κ,

$$\frac{T_c(\mu)}{T_c(\mu = 0)} = 1 - \kappa \left(\frac{N_c\mu}{T}\right)^2 + O\left[\left(\frac{N_c\mu}{T}\right)^4\right]. \quad (11)$$

For $T_c = T_\chi, T_\Phi$ and T_D with $\mu = \mu_{iso}$, the curvatures are obtained as $\kappa_\chi = 0.017 \pm 0.001$, $\kappa_\Phi = 0.004 \pm 0.001$ and $\kappa_D = 0.003 \pm 0.001$, respectively. Compared with the chiral transition, curvatures in T_Φ and T_D are much smaller, and show that the deconfinement temperature is much less sensitive to μ_{iso} than the chiral transition temperature. The chiral transition curvature is larger than the lattice result in the real quark chemical potential, $\kappa \simeq 0.008$ [24], but it is within the errorbar of the more recent lattice result $\kappa = 0.0149 \pm 0.0021$ [25]. The agreement would be accidental, but suggests the validity of the orbifold equivalence.

4. Summary

In this paper, we have discussed the deconfinement transition from topological viewpoints. Modification of the topology of

the system is achieved by introducing the dimensionless imaginary chemical potential (θ).

The topological difference between the confined and deconfined is visualized by using the map of the thermodynamic quantities to circle S^1 along periodic θ. Then, we find that there are three entangled rings of thermodynamic states in the deconfined phase, but there is only one ring in the confined phase after performing the 2-dimensional map of thermodynamic states. To understand it more clearly, we have considered three operations for the thermodynamic state, θ shift, the flux insertion to the closed Euclidean temporal coordinate loop and $\mathbb{Z}_{N_c}$ transformation, and found nontrivial commutation relations between them in the deconfined phase.

To investigate the topological deconfinement phase transition in the real chemical potential (μ_R) region, we have investigated the isospin chemical potential (μ_{iso}) region. Phase diagrams in both regions are identical to each other outside of the pion-condensed phase via the orbifold equivalence at least in the large-N_c limit. The chiral and pion condensates are strongly affected by μ_{iso}, but the Polyakov-loop and the quark number density at $\theta = \pi/3$ are not. We show this feature by estimating the curvature of transition lines. In the present PNJL model treatment, the gluonic part does not have explicit chemical potential dependence because the quark polarization effects are ignored. This leads to uncorrelated results between the chiral and deconfinement transitions. If we will access lattice QCD data of the quark number density at finite μ_{iso} with $\theta = \pi/3$ in the future, we can judge our surmise. If lattice simulations will provide the strong correlated results between the chiral and the deconfinement transitions at finite μ_{iso}, we can use the μ_{iso} region as a laboratory to extend the gluonic part of the effective model to include quark polarization effects by comparing the deconfinement transition in the effective model and that in lattice QCD simulations.

In this study, we clarify topological properties of QCD via the imaginary chemical potential. Also, it is a first study of the topological deconfinement transition at finite chemical potential. We hope that this study shed a light to nature of the deconfinement transition from topological viewpoint.

References

[1] M. Sato, Topological discrete algebra, ground state degeneracy, and quark confinement in QCD, Phys.Rev. D77 (2008) 045013. arXiv:0705.2476, doi:10.1103/PhysRevD.77.045013.

[2] X. Wen, Topological Order in Rigid States, Int.J.Mod.Phys. B4 (1990) 239. doi:10.1142/S0217979290000139.

[3] K. Kashiwa, A. Ohnishi, Topological feature and phase structure of QCD at complex chemical potential, Phys. Lett. B750 (2015) 282–286. arXiv:1505.06799, doi:10.1016/j.physletb.2015.09.036.

[4] A. Roberge, N. Weiss, Gauge Theories With Imaginary Chemical Potential and the Phases of QCD, Nucl.Phys. B275 (1986) 734. doi:10.1016/0550-3213(86)90582-1.

[5] K. Kashiwa, A. Ohnishi, Quark number holonomy and confinement-deconfinement transition, Phys. Rev. D93 (11) (2016) 116002. arXiv:1602.06037, doi:10.1103/PhysRevD.93.116002.

[6] M. D'Elia, F. Sanfilippo, The Order of the Roberge-Weiss endpoint (finite size transition) in QCD, Phys. Rev. D80 (2009) 111501. arXiv:0909.0254, doi:10.1103/PhysRevD.80.111501.

[7] C. Bonati, G. Cossu, M. D'Elia, F. Sanfilippo, The Roberge-Weiss endpoint in N_f = 2 QCD, Phys.Rev. D83 (2011) 054505. arXiv:1011.4515, doi:10.1103/PhysRevD.83.054505.

[8] K. Fukushima, Y. Hidaka, A Model study of the sign problem in the mean-field approximation, Phys.Rev. D75 (2007) 036002. arXiv:hep-ph/0610323, doi:10.1103/PhysRevD.75.036002.

[9] Y. Tanizaki, H. Nishimura, K. Kashiwa, Evading the sign problem in the mean-field approximation through Lefschetz-thimble path integral, Phys. Rev. D91 (10) (2015) 101701. arXiv:1504.02979, doi:10.1103/PhysRevD.91.101701.

[10] E. Witten, Analytic Continuation Of Chern-Simons Theory, AMS/IP Stud. Adv. Math. 50 (2011) 347–446. arXiv:1001.2933.

[11] M. Cristoforetti, F. Di Renzo, L. Scorzato, New approach to the sign problem in quantum field theories: High density QCD on a Lefschetz thimble, Phys.Rev. D86 (2012) 074506. arXiv:1205.3996, doi:10.1103/PhysRevD.86.074506.

[12] H. Fujii, D. Honda, M. Kato, Y. Kikukawa, S. Komatsu, T. Sano, Hybrid Monte Carlo on Lefschetz thimbles - A study of the residual sign problem, JHEP 1310 (2013) 147. arXiv:1309.4371, doi:10.1007/JHEP10(2013)147.

[13] A. Cherman, M. Hanada, D. Robles-Llana, Orbifold equivalence and the sign problem at finite baryon density, Phys. Rev. Lett. 106 (2011) 091603. arXiv:1009.1623, doi:10.1103/PhysRevLett.106.091603.

[14] A. Cherman, B. C. Tiburzi, Orbifold equivalence for finite density QCD and effective field theory, JHEP 06 (2011) 034. arXiv:1103.1639, doi:10.1007/JHEP06(2011)034.

[15] M. Hanada, N. Yamamoto, Universality of Phases in QCD and QCD-like Theories, JHEP 1202 (2012) 138. arXiv:1103.5480, doi:10.1007/JHEP02(2012)138.

[16] Y. Hidaka, N. Yamamoto, No-Go Theorem for Critical Phenomena in Large-Nc QCD, Phys.Rev.Lett. 108 (2012) 121601. arXiv:1110.3044, doi:10.1103/PhysRevLett.108.121601.

[17] K. Fukushima, Chiral effective model with the Polyakov loop, Phys.Lett. B591 (2004) 277–284. arXiv:hep-ph/0310121, doi:10.1016/j.physletb.2004.04.027.

[18] Y. Sakai, K. Kashiwa, H. Kouno, M. Yahiro, Polyakov loop extended NJL model with imaginary chemical potential, Phys.Rev. D77 (2008) 051901. arXiv:0801.0034, doi:10.1103/PhysRevD.77.051901.

[19] Z. Zhang, Y.-X. Liu, Coupling of pion condensate, chiral condensate and Polyakov loop in an extended NJL model, Phys. Rev. C75 (2007) 064910. arXiv:hep-ph/0610221, doi:10.1103/PhysRevC.75.064910.

[20] S. Roessner, C. Ratti, W. Weise, Polyakov loop, diquarks and the two-flavour phase diagram, Phys.Rev. D75 (2007) 034007. arXiv:hep-ph/0609281, doi:10.1103/PhysRevD.75.034007.

[21] H. Kouno, M. Kishikawa, T. Sasaki, Y. Sakai, M. Yahiro, Spontaneous parity and charge-conjugation violations at real isospin and imaginary baryon chemical potentials, Phys. Rev. D85 (2012) 016001. arXiv:1110.5187, doi:10.1103/PhysRevD.85.016001.

[22] S. Mukherjee, M. G. Mustafa, R. Ray, Thermodynamics of the PNJL model with nonzero baryon and isospin chemical potentials, Phys. Rev. D75 (2007) 094015. arXiv:hep-ph/0609249, doi:10.1103/PhysRevD.75.094015.

[23] J. Braun, H. Gies, J. M. Pawlowski, Quark Confinement from Color Confinement, Phys.Lett. B684 (2010) 262–267. arXiv:0708.2413, doi:10.1016/j.physletb.2010.01.009.

[24] C. R. Allton, S. Ejiri, S. J. Hands, O. Kaczmarek, F. Karsch, E. Laermann, C. Schmidt, L. Scorzato, The QCD thermal phase transition in the presence of a small chemical potential, Phys. Rev. D66 (2002) 074507. arXiv:hep-lat/0204010, doi:10.1103/PhysRevD.66.074507.

[25] R. Bellwied, S. Borsanyi, Z. Fodor, J. Gnther, S. D. Katz, C. Ratti, K. K. Szabo, The QCD phase diagram from analytic continuation, Phys. Lett. B751 (2015) 559–564. arXiv:1507.07510,